

Data example and modelling study of P-wave azimuthal anisotropy potentially caused by isotropic velocity heterogeneity

Edward Jenner¹

Abstract

Azimuthal variation in traveltimes is increasingly being used as a tool for reservoir characterization and fracture detection. One issue in interpreting the results of azimuthal normal moveout (NMO) analyses is to determine whether the apparent observed anisotropy is due to intrinsic azimuthal anisotropy or, in reality, is primarily caused by lateral velocity variations. A field data example is presented where lateral heterogeneity is suspected as the main cause of an observed azimuthal NMO anomaly. Modelling studies of isotropic media containing lateral velocity variations were performed to investigate the possibility that the observed anomaly in the field data could be caused solely by isotropic lateral velocity variation. In both the modelled and field data, the patterns observed in the apparent velocity anisotropy are very distinctive with obvious correlations between ellipse parameters (fast and slow velocities and azimuth of the fast velocity) and the structure of the lateral velocity variation. The inverted RMS and interval NMO ellipses also show a very high degree of correlation both spatially and temporally, extending below the heterogeneous layer.

Introduction

With the increasing interest in fractured reservoirs and characterization of general reservoir properties, azimuthal velocity analyses are becoming increasingly common (e.g., Al-Marzoug et al., 2006; Lynn, 2007; Tod et al., 2007). Within the range of offsets where the traveltimes are approximately hyperbolic, the azimuthal variation of pure-mode NMO velocity will be elliptical, independent of the subsurface geology (Grechka and Tsvankin, 1998). This is a nice feature from a processing standpoint, since one does not have to consider a specific geological model in data processing. However, for differentiating between even relatively simple models, such as one crack system versus two differently oriented crack systems, both P and S-wave data are required (e.g., Vasconcelos and Grechka, 2007).

For the interpreter, the ambiguity in interpreting P-wave NMO ellipses can be a significant problem in determining the geological model responsible for the observed azimuthal velocity variation. Not only may several anisotropic models fit the data, but apparent azimuthal variation in stacking velocity may also be caused by lateral velocity variations in an isotropic medium. In the case of relatively mild lateral velocity variations, the moveout may still be close to hyperbolic within a reasonable range of offsets. Within this offset range, and certainly within the constraints of noisy seismic data, the azimuthal variation in traveltimes may be indistinguishable from those caused by anisotropy. While Grechka and Tsvankin (1999) gave analytical results and a correction procedure to account for lateral velocity variations, this method makes assumptions about the nature, smoothness, and extent of the lateral velocity variation.

Strictly speaking, a non-linear lateral velocity variation will cause non-hyperbolic moveout at near to mid-offsets (at offsets less than the reflector depth) and fitting the azimuthal variation in velocity with an ellipse in this case is not appropriate. However, land data and even ocean bottom cable data are often quite noisy and deviations from hyperbolic moveout may not be obvious, especially when the overburden contains short-wavelength discrete lateral velocity variations. In this case, for any CMP gather, much of the moveout may be approximately hyperbolic, with some distortions in a certain offset range. In general, fitting these traveltimes in an azimuthal velocity analysis may result in significant apparent azimuthal velocity anisotropy where none exists.

In this paper a data example is presented that displays an azimuthal NMO velocity anomaly over an area of very mild structural dip where lateral velocity variation is the suspected culprit. This azimuthal NMO anomaly is strongly correlated with a stratigraphic feature, even after prestack time migration to collapse observed diffractions. The hypothesis that this azimuthal NMO anomaly may be caused by lateral velocity variation, rather than intrinsic anisotropy, is tested through modelling examples of lateral velocity variations embedded in an isotropic medium. Ray tracing is performed through these models and the derived traveltimes are inverted for the apparent azimuthal NMO. The modelling supports the hypothesis that the azimuthal NMO anomaly observed in the data example could be caused primarily by lateral velocity variation, rather than intrinsic anisotropy.

¹ ION Geophysical, 225 East 16th Ave, Suite 1200, Denver, CO80203, USA. E-mail: edward.jenner@iongeo.com

The method used for inverting traveltimes for azimuthal NMO for both the field and synthetic data was described in detail in Jenner (2001) and summarized by Jenner et al. (2001). It is a windowed cross-correlation technique that aims to provide relative trace-to-trace time shifts within a gather as a function of zero-offset traveltime. These time shifts are then used to compute total traveltimes as a function of offset at the chosen zero-offset times and inverted for the parameters defining the NMO ellipse (fast and slow velocities and direction of fast velocity) using the equations given by Grechka and Tsvankin (1998). Here anisotropy is defined as the difference between the fast and slow velocities divided by their average.

Data example

Figure 1 shows the seismic data example. The suspected region of lateral velocity variation is indicated by dashed ellipses in time slice, profile, and azimuthal NMO attributes of the prestack time-migrated (PSTM) data. Evidence for a potential lateral velocity variation comes from the change in structure and reflectivity. In addition, there is apparent time sag below the structure which also corresponds to a low velocity anomaly.

The background and overburden anisotropy is not expected to be zero and this results in the observed RMS and interval anisotropy (Figure 1b,c) and RMS and interval fast velocity magnitudes (Figure 1f,g). Outside the area of the suspected lateral velocity anomaly, the anisotropy does not appear to be correlated with the fast velocity magnitude. In addition, the RMS and interval parameters are not highly correlated in their spatial or temporal patterns. The low correlation is expected since RMS anisotropy should include the influence of the entire overburden, whereas the interval anisotropy should be local to the time interval of interest, subject to achievable vertical resolution. However, the elliptical pattern of high RMS anisotropy

marked by the ellipse in Figure 1b is also present in the interval anisotropy and both RMS and interval fast velocity. In addition, these patterns are also temporally correlated below the time shown. Both RMS (Figure 1h) and interval fast velocity directions are aligned perpendicular to the edge of the anomaly.

If this circular anomaly is caused by discrete lateral velocity variation, then one might suspect that the traveltimes would not fit the elliptical model for the variation in NMO velocity. The poor fit would then be indicative of lateral velocity variation, rather than anisotropy. One measure of the goodness of fit is the standard error computed from the least squares fitting of picked traveltimes. For the field data, a time slice through the error volume is shown in Figure 1d. While some acquisition footprint and areas of higher error are observed, there is no increase in the inversion error related to the area of suspected heterogeneity.

Synthetic model examples

Geological models were created and specular reflections from the horizontal interfaces were raytraced through the models. The acquisition geometry was a simple and regular square pattern with 300 m source and 150 m receiver group and line spacings. For the purposes of this experiment, and in the interests of time, diffractions were not modelled and consequently the data were not migrated prior to azimuthal velocity analysis. In addition, discontinuities in the models, non-zero ray capture radii and other numerical artefacts resulted in some errors being introduced into the traveltimes. Thus a small amount of noise is introduced into the models.

Results for three synthetic models are considered:

1. Wedge model. This is a model with a high-velocity wedge structure in the overburden. The resulting conclusions are applicable to both a low-velocity wedge in terms of azimuthal NMO response and changing the dip of the wedge.

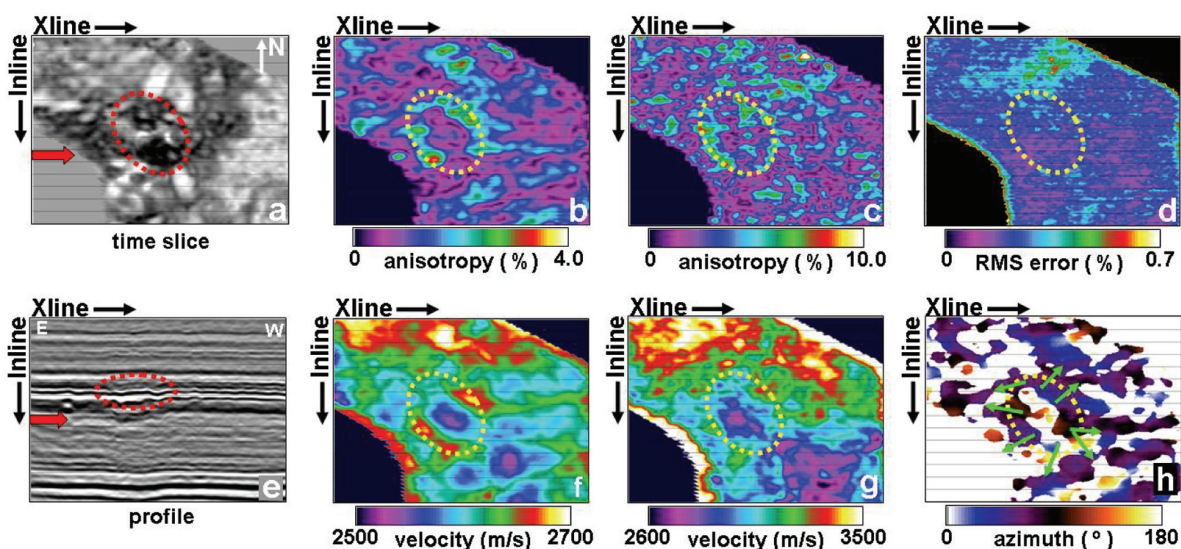


Figure 1 Field data example. (a) Time slice through velocity anomaly showing position of profile view (arrow) and extent of velocity anomaly. (b) Time-slice of RMS anisotropy. (c) Time-slice of interval anisotropy. (d) Error in RMS anisotropy. (e) Profile indicating area of velocity anomaly and position of time-slices. (f) Time-slice of RMS fast velocity. (g) Time-slice of interval fast velocity. (h) Azimuth of RMS fast velocity – only azimuths corresponding to high anisotropy are shown. Data courtesy of VGS Seismic.

2. Block model. This consists of a discrete, isotropic, rectangular block of higher velocity than the surrounding medium in the overburden. The block is large enough to be resolved both spatially and temporally with the frequency content of the synthetic seismograms.
3. Topographic model. An overburden containing a reflector with topography and velocity contrast with the overlying layer. This results in variable localized spatial lateral velocity variations whose azimuthal NMO imprints are superimposed upon each other.

Wedge model

Figure 2a shows the stack response for the 2.5D wedge model. The velocity structure is indicated in the figure and the dipping reflector is dipping to the east at 11°. Synthetic P-wave seismic data were generated from the horizontal reflectors. Using the method of Jenner (2001) and limiting the data to offset-to-depth ratios of 1.0, the resulting traveltimes were then picked and used to invert for the azimuthal velocity variation. Figure 2b shows a profile through the resulting apparent azimuthal anisotropy. The results of the inversion are two fan-shaped anisotropy anomalies centred at the east and west termination points of the lateral velocity variation.

These features can easily be explained by considering the azimuthal raypaths for reflections below the wedge. The N-S raypaths travel through the overburden with a different average velocity from the E-W rays. For the up-dip (eastern) anomaly the N-S direction averages a faster velocity (2250 m s⁻¹ for N-S rays) than the E-W direction. For the down-dip anomaly the N-S direction averages a slower velocity (2200 m s⁻¹). The azimuth of the fast velocity is shown in Figure 2c with 0° being N-S and 90° being E-W.

For CMP positions directly under the centre of the wedge the average velocity is the same in both the N-S and E-W directions. The traveltimes resulting in observed apparent anisotropy under the wedge do not strictly adhere to the elliptical variation in NMO velocity expected from an anisotropic medium. However, the net effect of inverting those traveltimes is an apparent azimuthal velocity response plus some noise. This model misfit noise can be observed as high-error regions in the traveltimes inversion.

Increasing the dip or velocity contrast of the wedge increases the magnitude but not the shape of the resulting apparent anisotropy. A low-velocity wedge will also create similar patterns of azimuthal anisotropy, but with the fast and slow velocity directions interchanged.

Figure 2d shows the anisotropy obtained after computing interval ellipses using the Dix-type method of Grechka et al. (1999). The apparent anisotropy is significant in magnitude, being approximately three times the magnitude of the RMS anisotropy. Perhaps more importantly from an interpretational perspective, the RMS and interval anisotropies have very similar temporal and spatial appearance. Note also that the interval anisotropy is not restricted to a region directly below the lateral velocity variation, as might be expected for a purely anisotropic layer.

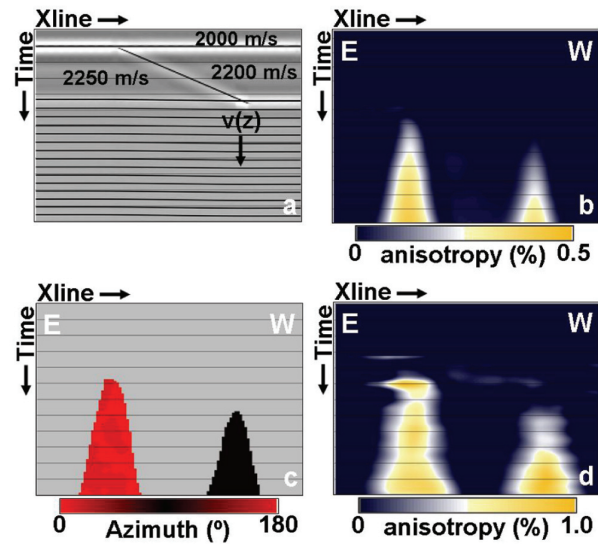


Figure 2 (a) East-west cross-section through stack of wedge model. (b) Resulting apparent RMS anisotropy. (c) Azimuths of fast velocity where NMO ellipticity is significant. (d) Interval anisotropy.

Block model

The second model considered is a 3D model and more closely resembles the structure of the data example. An isotropic rectangular block is embedded in a medium of slower velocity. Figure 3 shows results for this model. The anomaly is 1000 m wide in the N-S (inline) direction and 1800 m long in the E-W (crossline) direction, with ~10% variation in velocity between the high velocity block and surrounding medium.

Considering the simplicity of the model, the resulting apparent anisotropy is quite complex, with both lateral and vertical features. As with the wedge model, there is a high degree of temporal and spatial correlation between RMS and interval ellipses; however, this model also clearly demonstrates the similarity between the anisotropy and the variation in the fast velocity. Varying the size and shape, and adding anisotropy to the anomaly can have a significant impact on the details of the inverted NMO ellipses. Nevertheless, for the isotropic case the patterns and character of RMS and interval anisotropy have a high degree of correlation with each other and with the model heterogeneities. There is also high correlation between the other parameters defining the NMO ellipses (e.g., RMS anisotropy and fast velocity, or fast velocity and azimuth of the fast velocity) and between RMS and interval NMO ellipses. As with the wedge model, these correlations also extend below the heterogeneous layer and the RMS and interval fast velocity azimuths both align towards the centre of the anomaly.

Additional modelling, introducing anisotropy to the block, was also performed. It was observed that the correlation between parameters is particularly evident when the intrinsic anisotropy is small compared to the apparent anisotropy induced by the lateral velocity variations. As the intrinsic anisotropy is increased, the spatial and temporal correlations of the NMO ellipses below the block are reduced. However, as expected, at the time of the base reflection of the block,

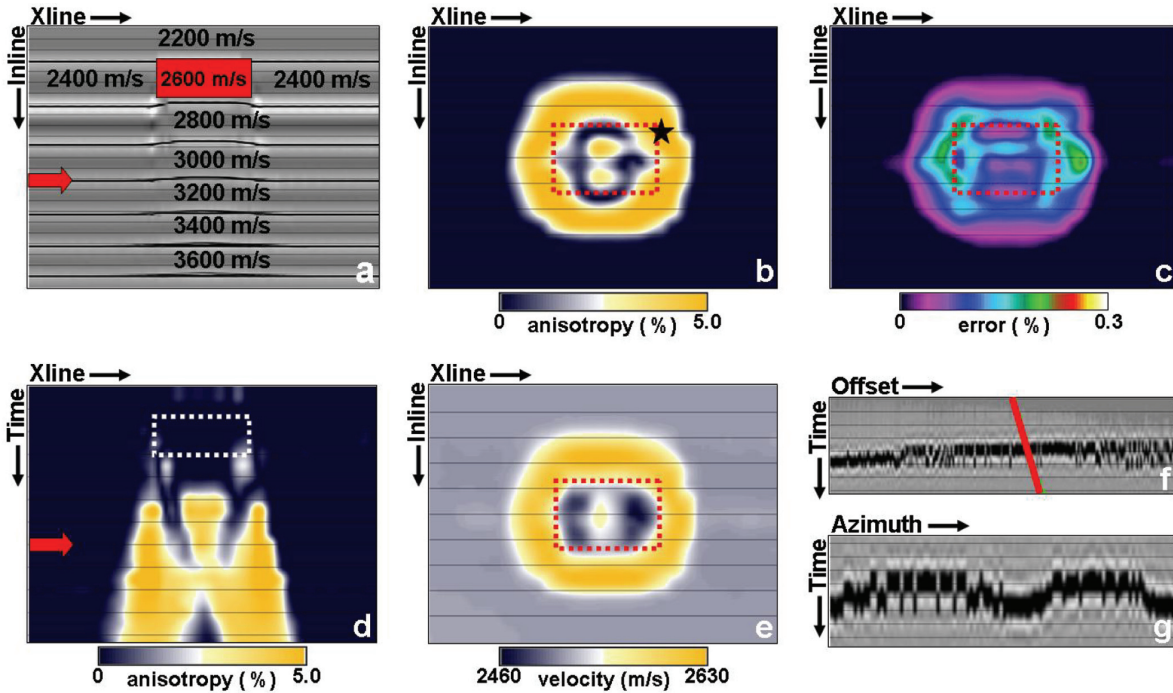


Figure 3 (a) Cross-section through block model showing position of time-slices. (b) Time-slice view of RMS anisotropy. (c) RMS error in the anisotropy. (d) Profile of RMS anisotropy showing position of time slices. (e) Time-slice view of the magnitude of the fast velocity. CMP supergather at position marked by the black star in (b) sorted as a function of (f) offset, where the red line indicates an offset-to-depth ratio of 1, and (g) source-receiver azimuth for offset-to-depth ratios of 0.6–0.8.

RMS and interval NMO ellipses are similar and the intrinsic anisotropy in the block is recovered.

The error volume (Figure 3c) computed from the least squares inversion of the picked traveltimes appears to be indicative of a problem with the inverted NMO ellipses. In any instance where the error shows the same patterns as the apparent anisotropy, one should be suspicious of the result. Usually, in field data this is indicative of areas of poorer acquisition geometry and lower signal-to-noise, where the acquisition geometry has driven the inversion result. In this case, however, it is due to the traveltimes not fitting the model for elliptical velocity variation.

The deviation in traveltimes from a homogeneous model as functions of offset and azimuth are illustrated in Figure 3f,g. The displayed CMP gather is located by the star in Figure 3b and has an isotropic NMO applied. As a function of offset (Figure 3f), one can observe non-hyperbolic and spurious traveltimes, even for offset-to-depth ratios of less than one. At the farther offsets, the reflection event clearly splits into two distinct traveltimes curves. These data have offset-to-depth ratios of 0.6–0.8 and are plotted as a function of source–receiver azimuth in Figure 3g without azimuth binning. In a narrow azimuth range, the reflection event appears at earlier or later times than expected for different, but close, offsets. Clearly this is due to the rays either travelling through the anomaly or, for a slightly different azimuth, missing it, and this causes the error in the inverted traveltimes seen in Figure 3c.

Taking a look at gathers across the anomaly shows how the traveltimes split into two distinct events (Figure 4). Rays travel-

ling though the anomaly arrive at earlier times and rays missing the anomaly arrive at later traveltimes. The least squares inversion of these traveltimes results in the somewhat complicated and not entirely predictable patterns of RMS anisotropy seen in Figure 3b,d. For this simple case, the spurious traveltimes seen in the CMP gathers could be used as an indication of lateral velocity variations rather than intrinsic azimuthal anisotropy.

However, this observation, as well as the discrete nature of the time shifts observed in Figure 3f,g, and thus the error shown in Figure 3c, is likely exaggerated because the raytracing technique used does not account for wavefront healing and finite frequency effects. Thus, for field data, the wavefield should not be expected to display such an obvious separation of traveltimes. This assertion is supported in the data example by the fact that the errors in the inversion are not correlated with the suspected lateral heterogeneity.

Topographic model

For the field data example, and in the general case, it is likely that the shape of any lateral velocity variation will be more complicated than the two models presented so far. To obtain some insight into what may be observed for more complex situations, a more general model of lateral velocity variation was considered. In this model topography was added to an overburden layer, with a velocity contrast with the surrounding medium, providing a significantly more complex pattern of lateral velocity variations. The modelled lateral heterogeneity and resulting RMS and interval anisotropy below the heterogeneous layer is shown in Figure 5. As with other models, increasing

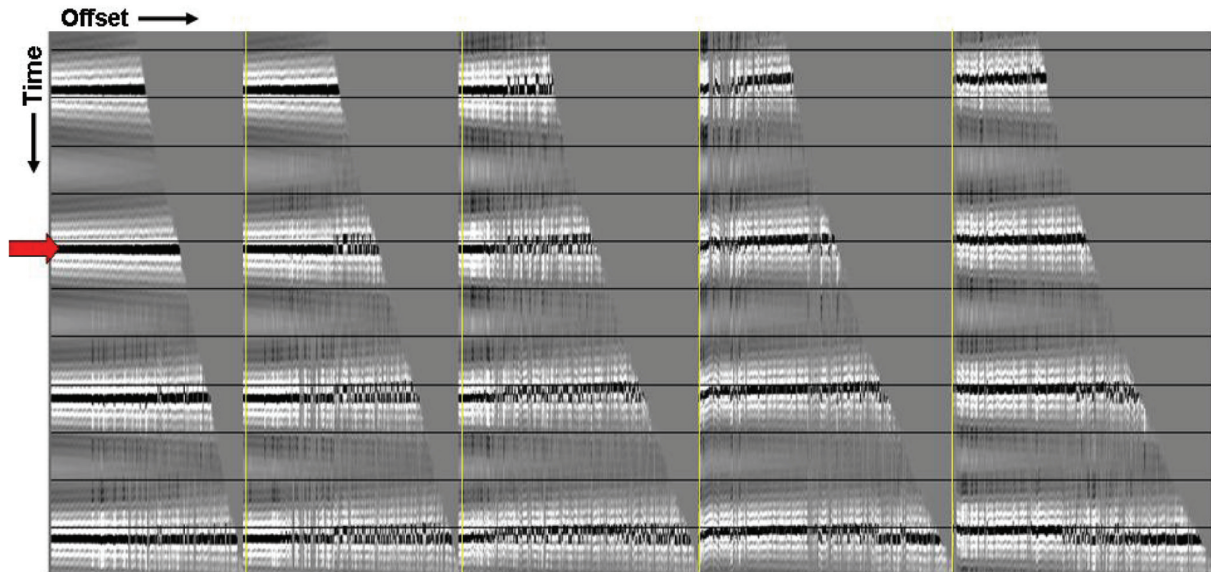


Figure 4 Five sample gathers across the anomaly, each sorted as a function of offset. The position of the time slices shown in Figure 3 is shown by the red arrow. Note how the traveltimes split into two distinct events, depending on whether the ray travels through the velocity anomaly or not. Offset range is from zero to approximately offset-to-depth ratios of 1.3.

the lateral variation results in increased apparent anisotropy, but does not change the degree of correlation between ellipse parameters. Below the heterogeneous layer the apparent anisotropy is rather complex (Figure 5c,d) and the variations in fast and slow velocities have very distinct patterns related to the topography (Figure 6).

In addition to being spatially correlated with the lateral velocity variations, the observed RMS and interval attribute patterns beneath the anomalous layer do not change appreciably with time. Thus, despite the complexity in the lateral heterogeneity, the RMS and interval NMO ellipses are spatially and temporally correlated, even significantly below the heterogeneous layer. The correlation is reflected in the similarity between RMS and interval anisotropy (Figure 5) and fast and slow velocities (Figure 6) at the reflection time indicated in Figure 5b. Thus the features observed for the simple models, namely correlation of NMO ellipses with the lateral heterogeneity and similarity of RMS and interval ellipses below the heterogeneous layers, are repeated for the more complex model.

For this model, the anisotropy is small enough that the errors in the inversion are closer to the magnitude of errors due to the acquisition geometry and inherent noise in the raytracing (Figure 7a). The subtle but regular N-S and E-W striping is due to the acquisition geometry (finite source and receiver spacing and errors in traveltimes). Superimposed upon the striping is the error due to the traveltimes not fitting the azimuthal velocity model. While the areas of highest error are not as clearly correlated with the individual attributes, they do still indicate that the highest errors are associated with the largest and most rapid lateral velocity changes in the model.

Unlike the previous example, however, CMP gathers in areas of high apparent anisotropy do not clearly show the influ-

ence of lateral velocity variation. Instead they simply appear to be contaminated with random traveltimes variations. Since there is no anisotropy in the model, one might expect the areas of highest apparent anisotropy to show the largest deviation in traveltimes, and hence largest error. However, this is clearly not the case (comparing Figures 7a and 5c). Figure 7 shows a CMP gather sorted as functions of offset (Figure 7b) and azimuth (Figure 7c) in an area of high anisotropy and relatively high error.

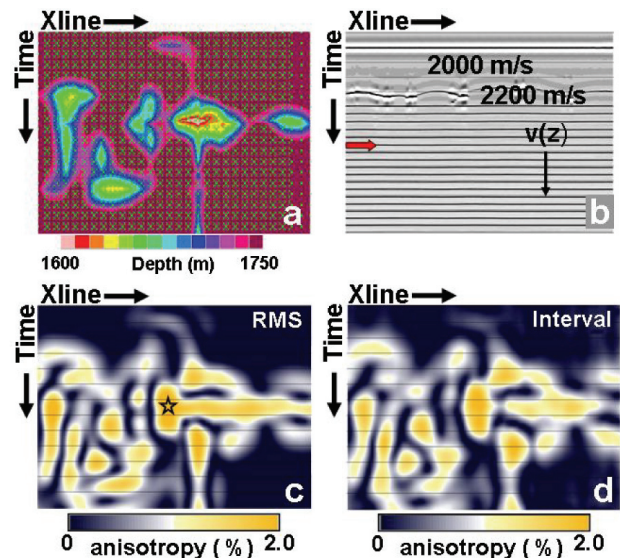


Figure 5 Displays of the more general, complex model showing lateral variations in velocity due to a contrast between a layer with topography and the overburden: (a) map of depths to layer, showing topography and hence shape of lateral velocity variation; (b) profile through a stack with time-slice positions indicated by red arrow; (c) time-slice of RMS anisotropy; and (d) time-slice of interval anisotropy. The star in (c) shows the location of the CMP gather displayed in Figure 7. The time slices are 600 ms below the base of the heterogeneous layer.

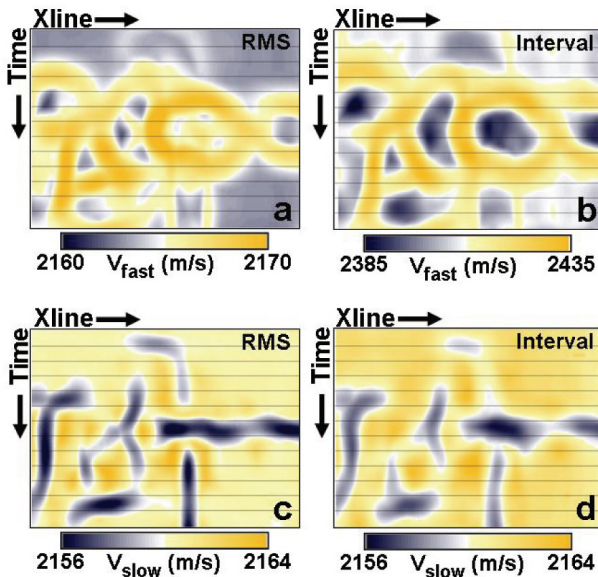


Figure 6 Time slices from the topographic model of (a) RMS fast velocity; (b) interval fast velocity; (c) RMS slow velocity; and (d) interval slow velocity. The time slices are 600 ms below the base of the heterogeneous layer and marked with the red arrow in Figure 5b.

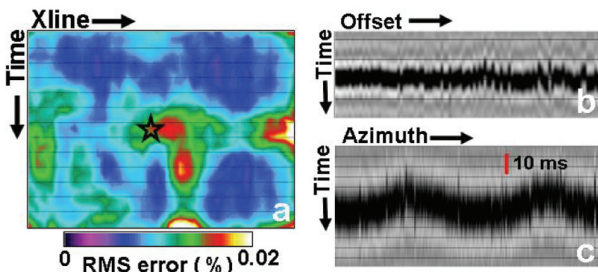


Figure 7 (a) RMS error in anisotropy. (b) Portion of a CMP gather at location marked by a star in (a) and in Figure 4c, sorted as a function of offset. (c) Portion of same CMP gather sorted as a function of source-receiver azimuth.

In essence, the complexity (lateral velocity variation) of the model has resulted in apparent anisotropy that would be indistinguishable from true anisotropy on CMP gathers, even those with a high signal to noise ratio. In addition, as with the previous examples, the raytracing does not account for wavefront healing and finite frequency of the seismic wavelet. Therefore, in field data one may not be able to distinguish complex lateral velocity variation from true anisotropy either by observing traveltimes on individual CMP gathers or analysis of inversion errors. This difficulty in making the distinction applied in the case of the field data example presented above (Figure 1d).

Conclusions

Non-linear lateral velocity variations can result in apparent azimuthal NMO velocity anisotropy, even if the medium is isotropic. In this paper a data example is presented where the primary cause of an azimuthal NMO anomaly may be lateral velocity variation. For this anomaly correlations are observed between inverted ellipse parameters (fast and slow

velocities and azimuthal of fast velocity) and also between RMS and interval NMO ellipses. The circular pattern of these anomalies also correlates with a stratigraphic feature. Modelling simple and more complex patterns of discrete lateral velocity variations within an isotropic medium results in inverted azimuthal NMO signatures that also display high degrees of spatial and temporal correlation with each other and the lateral heterogeneity. These correlations in ellipse parameters and RMS and interval NMO ellipses extend temporally, significantly below the velocity anomaly.

For the simplest models of lateral velocity variation and ignoring wavefront healing effects, errors in the traveltimes fitting can easily be observed on CMP gathers. However, as the model becomes more complex, deviations from the elliptical variation of NMO velocity are harder to distinguish, and standard errors computed from traveltimes inversion do not correlate as well with the lateral velocity variation. For field data, where noise is usually significant and acquisition geometries imperfect, there may be little correlation between the traveltimes fitting errors and subsurface structure.

Acknowledgements

The author is particularly grateful to VGS Seismic for permission to publish the field data example. In addition Robert Bloor and John Novak are thanked for their help and support and ION for permission to publish this work.

References

- Al-Marzoug, A.M., Neves, F.A., Kim, J.J. and Nebrija, E.L. [2006] P-wave anisotropy from azimuthal AVO and velocity estimates using 3D seismic data from Saudi Arabia. *Geophysics*, 71, E7-E11.
- Grechka, V. and Tsvankin, I. [1998] 3-D description of normal-moveout in anisotropic inhomogeneous media. *Geophysics*, 63, 1079-1072.
- Grechka, V. and Tsvankin, I. [1999] 3-D moveout inversion in azimuthally anisotropic media with lateral velocity variation: Theory and a case study. *Geophysics*, 64, 1202-1218.
- Grechka, V., Tsvankin, I. and Cohen, J. K. [1999] Generalized Dix equation and analytic treatment of normal-moveout velocity for anisotropic media. *Geophysical Prospecting*, 47, 117-148.
- Jenner, E. [2001] *Azimuthal Anisotropy of 3D Compressional Wave Seismic Data*. PhD thesis, Colorado School of Mines.
- Jenner, E., Williams, M. and Davis, T. [2001] A new method for azimuthal velocity analysis and application to a 3D survey, Weyburn Field, Saskatchewan, Canada. *71st SEG Annual Conference*, Expanded Abstracts, 102-105.
- Lynn, W. [2007] Uncertainty implications in azimuthal velocity analysis. *71st SEG Annual Conference*, Expanded Abstracts, 84-87.
- Tod, S., Taylor, B., Johnston, R. and Allen, T. [2007] Fracture prediction from wide-azimuth land seismic data in SE Algeria. *The Leading Edge*, 26, 1154-1160.
- Vasconcelos, I. and Grechka, V. [2007] Seismic characterization of multiple fracture sets at Rulison Field, Colorado. *Geophysics*, 72, B19-B30.

Received 17 October 2008; accepted 22 December 2008.